

# Broad-band X-Ray Spectra of the Black Hole Candidate GRO J1655–40

John A. Tomsick<sup>1</sup>, Philip Kaaret<sup>1,4</sup>, Richard A. Kroeger<sup>2</sup>, Ronald A. Remillard<sup>3</sup>

## ABSTRACT

We present broad-band (2 keV to 2 MeV) x-ray spectra of GRO J1655–40, a luminous X-ray transient and occasional source of relativistic radio jets, obtained with the *Rossi X-Ray Timing Explorer* (RXTE) and the Oriented Scintillation Spectrometer Experiment (OSSE). In one observation, the luminosity is found to be 18% of the Eddington limit, which is one of the highest luminosities ever observed from GRO J1655–40. For this observation, we find that an adequate fit is obtained when a broad iron line and a reflection component are added to a model consisting of a power-law plus a soft excess component. The 95% confidence lower limit on the rms line width is 0.86 keV. The power-law component has a photon index of  $2.72_{-0.08}^{+0.03}$  and extends to at least 800 keV without a cutoff.

After this observation, a significant drop in the (5–12 keV)/(1.5–5 keV) hardness ratio occurred on a timescale less than 2 hours. From an RXTE observation of GRO J1655–40 made after the hardness transition, we find that the power-law index is harder ( $\alpha = 2.415 \pm 0.011$ ), the flux of the power-law component is lower, and the total luminosity is 10% of the Eddington limit. The change in the power-law component is consistent with the correlation between the spectral index and power-law flux previously reported for GRO J1655–40.

*Subject headings:* accretion, accretion disks — BHXNe: general — stars: individual (GRO J1655–40) — stars: black holes — X-rays: stars

---

<sup>1</sup>Department of Physics and Columbia Astrophysics Laboratory, Columbia University, 550 W. 120th Street, New York, NY 10027

<sup>2</sup>Naval Research Laboratory, Code 7650, Washington DC

<sup>3</sup>Center for Space Research, Massachusetts Institute of Technology, Cambridge, MA 02139

<sup>4</sup>Current address: Harvard-Smithsonian Center for Astrophysics, 60 Garden Street, Cambridge, MA 02139 (e-mail: pkaaret@cfa.harvard.edu)

## 1. Introduction

The X-ray transient GRO J1655–40 was discovered with the Burst and Transient Source Experiment (BATSE) on the *Compton Gamma-Ray Observatory* (CGRO) on July 27, 1994 (Zhang et al. 1994). GRO J1655–40 is often called a microquasar because radio jets moving at 92% of the speed of light relative to the X-ray source have been observed (Tingay et al. 1995; Hjellming & Rupen 1995). From optical measurements made in X-ray quiescence, the compact object mass and the orbital inclination have been found to be  $7.02 \pm 0.22 M_{\odot}$  and  $69.50 \pm 0.08$  degrees, respectively (Orosz & Bailyn 1997). These are the most precise compact object mass and orbital inclination measurements which have been made for any black hole candidate, which makes GRO J1655–40 an excellent laboratory for learning about accreting black holes.

Since the discovery of GRO J1655–40, its 20–200 keV X-ray flux has been monitored by BATSE (Tavani et al. 1996). In the BATSE bandpass, a power-law spectrum is observed with a photon index varying between 1.8 and 3.1. The BATSE data suggest that the photon index softens as the source intensity increases (Wilson et al. 1995; Zhang et al. 1995). This trend has also been reported from observations of GRO J1655–40 by the Oriented Scintillation Spectrometer Experiment (OSSE) on CGRO (Grove et al. 1998). OSSE measurements of GRO J1655–40 have been made between August 1994 and September 1996. During observations where the source was detected, the spectrum in the OSSE bandpass is consistent with a power-law (Kroeger et al. 1996; Grove et al. 1998). In this paper, we report on simultaneous RXTE and OSSE observations of GRO J1655–40 made in 1996. Soft X-ray measurements of the source made with the *Advanced Satellite for Cosmology and Astrophysics* (ASCA) indicate the presence of an ultrasoft component (Zhang et al. 1997a), which probably comes from an accretion disk around the compact object.

Previous spectral and timing measurements of GRO J1655–40 have been interpreted as evidence that the compact object in this system is a rapidly rotating black hole (Zhang, Cui & Chen 1997b; Cui, Zhang, & Chen 1998a). Similar results have been obtained for another microquasar, GRS 1915+105, suggesting that the relativistic, highly collimated radio jets in the microquasars are related to the presence of a rapidly rotating black hole (Zhang et al. 1997b). Black hole rotation rate has long been considered as a way to explain the radio loud/radio quiet dichotomy in AGN (Wilson & Colbert 1995).

In this paper, we report on simultaneous observations of GRO J1655–40 made by the *Rossi X-Ray Timing Explorer* (RXTE) and OSSE. After describing the observations and our analysis techniques, we present the results of the spectral fits. We then discuss the results and end with our conclusions.

## 2. Observations

Figure 1 shows the GRO J1655–40 RXTE All-Sky Monitor (ASM) light curve and (5–12 keV)/(1.5–5 keV) hardness ratio from late August to early September 1996 when GRO J1655–40 was observed simultaneously with RXTE and OSSE. OSSE observations were made following observations by BATSE indicating that GRO J1655–40 had undergone several strong outbursts since mid-July 1996. The decision to observe GRO J1655–40 came during the fifth outburst of this series above 1 Crab in the 20–100 keV energy band. These RXTE and OSSE observations occur during one of the highest luminosity and hardest states of GRO J1655–40 (Remillard et al. 1998). A sharp change in the ASM hardness is seen at MJD 50328.5, which is marked with a vertical dotted line in Figure 1. For the six days before the transition, the ASM count rate is constant (in 1-day averages) to  $\pm 6\%$  with a mean value of  $220 \pm 2 \text{ s}^{-1}$ , corresponding to about 2.9 Crab. Over the same time period, the mean hardness ratio is  $0.449 \pm 0.003$ . At the transition, the

hardness changes on a timescale less than 2 hours, while the 1.5-12 keV flux dips sharply, recovers, and then decays to a constant level in about 1.5 days. During the time from MJD 50330 to MJD 50335, the mean ASM count rate is  $170 \pm 1 \text{ s}^{-1}$  and the one day averages vary by  $\pm 4\%$ . The OSSE observation was made from MJD 50322.4 to MJD 50328.4 and lies completely in the time interval of high X-ray hardness. Pointed RXTE observations, marked with arrows in Figure 1b, were made on MJD 50324.4 and MJD 50330.3. One RXTE observation is during the OSSE observation and the other is after the hardness transition. The first RXTE observation contains 4334 s of PCA livetime and 2929 s of HEXTE livetime (on source). The second RXTE observation contains 5618 s of PCA livetime and 3715 s of HEXTE livetime.

GRO J1655–40 radio observations were made with the *Very Large Array* (VLA) and the *Molonglo Observatory Synthesis Telescope* (MOST) close to the time of the RXTE and OSSE observations (R.M. Hjellming & R. Hunstead, private communication). GRO J1655–40 was not detected for any of the radio observations. Observations were made by the VLA on MJD 50323, 50326, 50330, and 50337 resulting in upper limits of 0.4 mJy, and observations were made by MOST on MJD 50306, 50313, 50326, and 50340 resulting in an upper limit of 4 mJy.

### 3. Analysis

PCA energy spectra have been produced using Standard 2 PCA data and the Version 2.2.1 (January 20, 1998) response matrix (Jahoda et al. 1997). During the pre-transition observation, Proportional Counter Unit (PCU) 3 was off. To test the PCA response matrix for the remaining PCUs (0, 1, 2, and 4), we fit the Crab spectrum with a power-law. Crab spectra have been extracted from an 11.6 ks observation made between MJD 50529.9 and 50530.2. We produced spectra containing data from all three xenon layers and also from only the top xenon layer. In both cases, power-law fits to the Crab are significantly better for PCUs 0, 1, and 4 than for PCU 2. Also, the top layer spectra give column densities and photon indices which are closer to the conventional values for the Crab (Toor & Seward 1974; Koyama et al. 1984; Schattenburg & Canizares 1986; Turner et al. 1989) than the spectra for all three layers combined. Thus, the GRO J1655–40 spectral analysis has been performed using events from the top layers of PCUs 0, 1, and 4. Although PCU 3 was on during the post-transition observation, it has not been used in order to avoid instrumental differences between the pre-transition and post-transition spectra. A systematic error of 1% is assumed to account for uncertainties in the response matrix, and the normalizations have been left free between PCUs. Spectral bins from 2.5 keV to 20.0 keV have been used for the spectral analysis. Background subtraction has been performed including estimates for the particle, X-ray, and activation background spectra (Stark et al. 1997); however, for both spectra, activation does not contribute to the background. The spectra have been corrected for deadtime.

We find that pile-up has a significant impact on the GRO J1655–40 PCA spectrum. The ratio of the pile-up spectrum to the measured spectrum reaches a maximum of 5% near 18 keV for the pre-transition spectrum, while the ratio reaches a maximum of 5% near 13 keV for the post-transition spectrum. Thus, a correction for pile-up has been applied as described in Tomsick & Kaaret (1998).

HEXTE energy spectra have been produced using Standard mode data, which consist of 64-bin spectra with 16 s time resolution. The March 20, 1997 HEXTE response matrices have been used. For HEXTE, it is essential to correct for deadtime (Rothschild et al. 1997), and this correction has been made. For the spectral fits, the normalizations have been left free between cluster A and cluster B.

OSSE made its standard observation over a period of six days by pointing its collimator at GRO J1655–

40, and comparing this with count rates in background fields 4.5 degrees on either side of the source. Due to the large field of view of OSSE,  $3.8^\circ$  by  $11.4^\circ$  full width at half maximum response, the observations have potential problems with source confusion. Nearby sources 4U 1700–37 and OAO 1657–415 are not significant sources above 100 keV in comparison to GRO J1655–40 and can be ignored. To make sure that the OSSE data is not contaminated due to source confusion, we compared the OSSE spectrum to the HEXTE spectrum in the energy band where the two instruments overlap. We find that the OSSE and HEXTE spectra are consistent, up to a constant normalization factor, in this energy band. Narrow-line annihilation radiation from the galactic plane could potentially be a source of contamination; however, for this observation, the orientation of the spacecraft was chosen to minimize this contamination. No evidence for 511 keV line emission from GRO J1655–40 was detected in these observations.

The normalizations between the PCA, HEXTE, and OSSE have been left free. To estimate the GRO J1655–40 flux, we have compared the Crab nebula flux measured by the PCA to previous measurements of the Crab flux by other instruments (Toor & Seward 1974; Koyama et al. 1984; Schattenburg & Canizares 1986; Turner et al. 1989). We find that PCUs 0, 1, and 4 measure 2.5 to 25 keV Crab fluxes of 3.43, 3.38, and  $3.29 (\pm 0.05)$  photons  $\text{cm}^{-2} \text{s}^{-1}$ , respectively, while previous measurements give  $2.91 \pm 0.03$  photons  $\text{cm}^{-2} \text{s}^{-1}$  in the same energy band. When fluxes or spectral component normalizations are given in this paper, they have been reduced by a factor of 1.18 so that the PCA flux scale is in agreement with previous instruments. Spectral fits have been calculated using the version 10 XSPEC software (Shafer et al. 1991).

#### 4. Spectral Results

We first fit the pre-transition GRO J1655–40 HEXTE and OSSE spectra without the data from the PCA. Since a power-law does not provide an acceptable fit ( $\chi^2/\nu = 197/140$ ), more complicated models were used to improve the fit. The fit results are shown in Table 1. A model consisting of a power-law with an exponential break (cutoff power-law) gives  $\chi^2/\nu = 149/139$ , which is a significant improvement over a power-law. The photon index and folding energy are found to be  $2.703 \pm 0.010$  and  $1086_{-145}^{+195}$  keV, respectively. The error estimates given here and throughout the text are 68% confidence for one interesting parameter ( $\Delta\chi^2 = 1.0$ ). A similar improvement is observed using a model consisting of a power-law with a reflection component (Magdziarz & Zdziarski 1995). For this fit, we fixed the inclination angle to  $69.5^\circ$ , which is the binary inclination angle measured by Orosz & Bailyn (1997), and assumed that the reflecting material has cosmic abundances. We find that the photon index and covering fraction ( $\Omega/2\pi$ ) are  $2.739 \pm 0.006$  and  $0.396 \pm 0.065$ , respectively, and that the spectral shape is consistent with the reflecting material being unionized. A broken power-law with a break at  $63_{-14}^{+9}$  keV also provides a good fit to the data. The photon indices for this fit are shown in Table 1.

When the PCA data is added to the pre-transition spectrum, a soft excess is observed, which is probably due to emission from an accretion disk. We first use a disk-blackbody component (Makishima et al. 1986) to model the soft excess. The disk-blackbody model we use is not standard in XSPEC version 10. The difference between our model and the standard XSPEC disk-blackbody model (“diskbb”) is that we use the relation between temperature and radius is given in equation (3.23) of Pringle (1981). For our model, which is described in more detail in Tomsick et al. (1998), the spectrum is determined by the normalization,  $N_{DBB}$ , and the maximum disk color temperature,  $T_{max}$ . The normalization is given by

$$N_{DBB} = \frac{\cos i}{f^4} \left( \frac{R_{in}/1 \text{ km}}{d/10 \text{ kpc}} \right)^2, \quad (1)$$

where  $i$  is the disk inclination,  $f$  is the color correction factor,  $R_{in}$  is the inner radius of the disk, and  $d$  is the distance to the source. In the following, we assume that  $f = 1.7 \pm 0.2$  (Shimura & Takahara 1995; Zhang et al. 1997b) and that  $d = 3.2 \pm 0.2$  (Hjellming & Rupen 1995). We also model the soft excess using a Comptonization component (Sunyaev & Titarchuk 1980) rather than the disk-blackbody. The Comptonization model approximates the situation where soft X-rays from the accretion disk are upscattered in a plasma above the accretion disk. It is important to note that the Comptonization model we use only applies if the plasma is relatively optically thick ( $\tau > 3$ ) and the electrons in the plasma are non-relativistic (i.e.  $kT_e \ll m_e c^2$ ). After the spectra are fit using this Comptonization model, it will be necessary to check that the fit parameters satisfy these conditions. A disk-blackbody plus power-law model does not provide a formally acceptable fit to the pre-transition spectrum ( $\chi^2/\nu = 391/274$ ). A Comptonization plus power-law model provides a significantly better fit; however, it is still not formally acceptable ( $\chi^2/\nu = 291/273$ ). As shown in Figures 2a and 2b, significant systematic features are seen in the residuals for both models.

To see if the systematic features in the GRO J1655–40 residuals are due to problems with understanding the instrument responses, we produced PCA and HEXTE Crab spectra. To make the spectra, we used data from the 11.6 ks Crab observation mentioned previously. The Crab spectra were created using the same procedures as for the GRO J1655–40 data. We note that only top layer PCA data are used. The Crab spectra and the residuals for a broken power-law fit are shown in Figure 3. The data is well fit with a broken power-law ( $\chi^2/\nu = 146/221$ ). The systematic features that are observed in the GRO J1655–40 residuals are not seen in the Crab residuals; thus, we assume that the features in the GRO J1655–40 residuals are not due to problems in understanding the instrument responses.

The positive residuals in the pre-transition spectrum between 6 and 8 keV suggest the presence of an iron line. Since an iron line is expected if reflection is being observed, we choose to model the high energy portion of the spectrum using a power-law with a reflection component. Thus, in the following, we use a model consisting of a soft component (disk-blackbody or Comptonization), a gaussian emission line, and a power-law with a reflection component to fit the GRO J1655–40 spectra. As shown in Tables 2 and 3, similar results are obtained using the disk-blackbody model and the Comptonization model. Specifically, we find that both reflection and the gaussian emission line are necessary at more than 99% significance. Henceforth, Model 1 will refer to a model consisting of a disk-blackbody, a gaussian emission line, a power-law, and reflection, and Model 2 will refer to a model consisting of a Comptonization component, a gaussian emission line, a power-law, and reflection.

The fit parameters for the Model 1 and Model 2 fits to the pre-transition spectrum are shown in Tables 4 and 5, respectively. For the reflection component, we measure a covering fraction of  $0.259_{-0.053}^{+0.054}$  using Model 1 and  $0.85_{-0.25}^{+0.68}$  using Model 2. Using Model 1, we find that the iron line centroid ( $E_{line}$ ) is  $6.81_{-0.31}^{+0.24}$  keV, and that the equivalent width is 113 eV. For Model 2,  $E_{line} = 6.21_{-0.33}^{+0.31}$  keV and the equivalent width is 319 eV. In both cases, the line is very broad. The 95% confidence lower limit ( $\Delta\chi^2 = 4.0$ ) on the width of the line ( $\sigma_{line}$ ) is 0.86 keV and 1.42 keV for Models 1 and 2, respectively. The residuals for pre-transition Model 1 and Model 2 fits are shown in Figures 2c and 2d, respectively, and the pre-transition spectrum, fit using Model 1, is shown in Figure 4a. For both models, the iron line centroid does not constrain the ionization state of the reflecting material. Thus, to constrain the ionization state of the material, we freed the ionization parameter ( $\xi$ ) in the reflection model and, assuming a disk temperature of  $10^5$  K (Cui et al. 1998b), we refit the spectra. For Model 1 and Model 2, we find that the best value for  $\xi$  is 0.0, and, for this parameter, we derive 95% confidence upper limits on  $\xi$  of  $1380 \text{ erg cm s}^{-1}$  and  $48 \text{ erg cm s}^{-1}$  for Model 1 and Model 2, respectively. Although the spectrum is consistent with the reflecting material being unionized,  $\xi$  is not very well constrained. The fact that  $\xi$  is not well constrained

is not surprising because of the presence of the broad iron line. For Model 2, we find that the conditions for the validity of the Comptonization model are met. Specifically, we find that  $\tau = 7.64_{-0.65}^{+0.75}$  and that the Comptonization component is responsible for less than 1% of the flux for all energies greater than 28 keV, indicating that relativistic corrections to this model are not significant in this case.

When the post-transition spectrum is fit with a disk-blackbody plus power-law model, the fit is formally acceptable ( $\chi^2/\nu = 187/221$ ). However, as for the pre-transition spectrum, we tried to improve the fit using a reflection component and a gaussian line. As shown in Table 2, we find that including a reflection component improves the fit only slightly. Adding a gaussian iron line improves the fit significantly, and we find that this component is necessary at more than 99% significance. Further evidence that the reflection component is not necessary to fit the post-transition spectrum comes from the fact that adding a reflection component to a model consisting of a disk-blackbody, a gaussian iron line, and a power-law does not improve the fit. As shown in Table 3, similar results are obtained using the Comptonization model instead of the disk-blackbody. Specifically, we find that the gaussian iron line is necessary at more than 99% significance, but there is no evidence for reflection.

The fit parameters for the Model 1 and Model 2 fits to the post-transition spectrum are shown in Tables 4 and 5, respectively. For the post-transition fits described above, all three gaussian iron line fit parameters were left as free parameters. However, we find that for both Model 1 and Model 2, the post-transition values found for  $E_{line}$  and  $\sigma_{line}$  are consistent with those found for the pre-transition fits. Thus, the post-transition fits were recalculated after fixing  $E_{line}$  and  $\sigma_{line}$  to the pre-transition values in order to improve the constraints on the other parameters. For both models, we find that the equivalent width of the iron line is lower for the post-transition spectrum than for the pre-transition. For Model 1, the equivalent width is 38 eV, and for Model 2, the equivalent width is 192 eV. We also place upper limits on the covering fraction for reflection. Using Model 1, we find that the 95% confidence upper limit on  $\Omega/2\pi$  is 0.067, while using Model 2 the 95% confidence upper limit is 0.15. Thus, reflection is significantly less important in the post-transition spectrum compared to the pre-transition spectrum. Another significant difference between the spectra, which will be discussed further below, is that the power-law index for the post-transition spectrum is considerably harder than for the pre-transition spectrum. The post-transition spectrum, fit using Model 1, is shown in Figure 4b.

ASCA observations of GRO J1655-40 give column densities ranging from  $N_H = 4.4 \times 10^{21} \text{ cm}^{-2}$  (Nagase et al. 1994) to  $N_H = 8.9 \times 10^{21} \text{ cm}^{-2}$  (Zhang et al. 1997a). Fitting the pre-transition spectrum with Model 1 gives a column density which is significantly above this range (cf. Table 4). To check this result, we fixed  $N_H$  to the value found by Zhang et al. (1997a) and refit the pre-transition spectrum using Model 1. With  $N_H$  fixed, we find that  $\chi^2/\nu = 293/272$ , which is significantly worse than the fit with  $N_H$  free. The column density for the pre-transition spectrum may be higher than the previous values found using ASCA and higher than we find for the post-transition spectrum because of absorption due to material near the source. When Model 2 is used, the column densities for the pre-transition and post-transition spectra are consistent (cf. Table 5). Although the values of  $N_H$  found using Model 2 are above the range of values found using ASCA, the ASCA column densities are derived using different spectral models.

From ASCA spectra, Ueda et al. (1998) recently reported a detection of iron absorption lines for GRO J1655-40. In the August 1995 ASCA spectrum, Ueda et al. (1998) find a  $K\alpha$  absorption line due to highly ionized iron (Fe XXVI) with an equivalent width of  $25_{-11}^{+13}$  eV. Ueda et al. (1998) derives a  $1-\sigma$  upper limit on the width of the iron line of 150 eV. To look for this absorption line in our spectra, we added a gaussian at a fixed energy of 6.98 keV and a fixed width of 150 eV to Model 1 and refit the pre-transition and post-transition spectra. An absorption line is not detected for either the pre-transition

or post-transition spectrum. For the pre-transition spectrum, we find a 95% confidence upper limit on the equivalent width of 24.4 eV, and for the post-transition spectrum, we find a 95% confidence upper limit on the equivalent width of 26.5 eV. Although we do not detect an iron absorption line, our data does not allow us to rule out the absorption line observed by Ueda et al. (1998). However, it appears that the structure between 6 and 8 keV in our spectrum is considerably different from that observed by ASCA since we observe an iron emission line that was not detected by ASCA.

## 5. Discussion

For GRO J1655–40, the change from the pre-transition state to the post-transition state represents a significant change in the luminosity, and hereafter the pre-transition state will be referred to as the high-luminosity state and the post-transition state will be referred to as the intermediate-luminosity state. The unabsorbed luminosity for the high-luminosity state is  $1.7 \times 10^{38}$  erg s<sup>-1</sup> (1.5 keV to 2 MeV), assuming a distance of 3.2 kpc and isotropic emission, corresponding to 18% of the Eddington luminosity ( $L_{edd}$ ) for a  $7M_{\odot}$  compact object (Orosz & Bailyn 1997). For the intermediate-luminosity state, the unabsorbed luminosity is  $9.2 \times 10^{37}$  erg s<sup>-1</sup> (1.5 keV to 2 MeV), which is 10% of  $L_{edd}$ . Figure 5 shows the high-luminosity and intermediate-luminosity state spectra along with a previously reported GRO J1655–40 broad-band spectrum based on simultaneous August 1995 ASCA and BATSE observations (Zhang et al. 1997a). The intermediate-luminosity state spectrum is very similar to the August 1995 spectrum, while the shape of the high-luminosity state spectrum is much different.

For the power-law component, the intermediate-luminosity state photon index is considerably harder than the high-luminosity state photon index ( $\alpha = 2.415 \pm 0.011$  compared to  $\alpha = 2.72_{-0.08}^{+0.03}$ ). Also, the 2.5 keV to 2 MeV flux of the power-law component is about a factor of three higher for the high-luminosity state than the intermediate-luminosity state. The differences in the power-law component between the high-luminosity and intermediate-luminosity state are consistent with the trend previously reported for GRO J1655–40 by Wilson et al. (1995) from BATSE measurements and by Grove et al. (1998) from OSSE measurements that the spectral index softens as the intensity of the hard component increases.

Chakrabarti & Titarchuk (1995) have suggested that the power-law component may be caused by the Comptonization of soft photons from the accretion disk by material being radially accreted onto the black hole. This mechanism, known as bulk-motion Comptonization, is different from thermal Comptonization models (e.g. Titarchuk 1994) since it relies on the radial velocity of the infalling material to produce hard x-rays. The bulk-motion Comptonization model predicts a cutoff in the spectrum at  $E \lesssim m_e c^2$  (Shrader & Titarchuk 1998). In Table 1, we show that a power-law with a spectral cutoff provides a better fit to the high-luminosity spectrum than a power-law with no cutoff. However, the measured cutoff energy of  $1086_{-145}^{+195}$  keV is considerably higher than 511 keV ( $m_e c^2$ ). We find that the 95% confidence lower limit to the cutoff energy is 829 keV.

To explain the GRO J1655–40 hard component, it is necessary to explain the lack of a cutoff in the spectrum below about 800 keV and the correlation between flux and power-law index. The flux-index correlation is commonly seen in AGN (Grandi et al. 1992; Guainazzi et al. 1996), and has been explained by inverse Compton scattering of soft photons on hot electrons with a thermal velocity distribution (Haardt, Maraschi, & Ghisellini 1997) or on electrons with a non-thermal velocity distribution (Yaqoob 1992). However, it should be noted that the typical photon index observed for AGN is significantly harder than for GRO J1655–40 and that the high energy cutoffs observed in AGN are well below  $m_e c^2$ .

While the behavior of the power-law component does not depend on whether Model 1 or Model 2 is used, the change in the soft component does depend on which model is used. As shown in Table 4, if Model 1 is used, the flux of the disk-blackbody component is about a factor of two higher in the intermediate-luminosity state than in the high-luminosity state. If Model 2 is used, the flux of the Comptonization component does not change significantly between states (cf. Table 5).

Although Model 1 and Model 2 provide acceptable fits to both spectra, the models are based on somewhat different physical assumptions. The main difference is that while Model 1 assumes that we are seeing blackbody emission from an optically thick disk directly, Model 2 assumes that we see the soft emission from the disk only after it is Comptonized, possibly in an accretion disk corona. The Comptonization parameters we give in Table 5 assume a disk geometry for the Comptonization region. In the following, we first discuss the results assuming Model 1 correctly describes the physical situation, then we will discuss the results assuming the physical situation is correctly described by Model 2.

### 5.1. Model 1 Implications

From analysis of the August 1995 GRO J1655–40 spectrum, which is similar to our intermediate-luminosity state spectrum, Zhang, Cui, & Chen (1997b) suggest that the black hole in GRO J1655–40 is rotating at about 93% of its maximal rate in the prograde direction (i.e.  $a_* = 0.93$ ). We define  $a_* = a/r_g$  where  $a = J/Mc$ ,  $r_g = GM/c^2$ , and  $M$  and  $J$  are the mass and the angular momentum of the black hole, respectively. In their calculation, Zhang et al. (1997b) assume that the disk extends to the marginally stable orbit,  $r_{ms}$ . When Model 1 is used to fit the GRO J1655–40 spectra, the disk-blackbody parameters imply that the inner edge of the disk is closer to the compact object in the high-luminosity state than in the intermediate-luminosity state. This may indicate that the inner edge of the disk in the intermediate-luminosity state does not reach  $r_{ms}$ . Also, since  $r_{ms}$  decreases with increasing black hole rotation rate, our spectral results for the high-luminosity state imply that  $a_* > 0.93$ . The inner disk radius ( $R_{in}$ ) can be derived from the disk-blackbody normalizations ( $N_{DBB}$ ) using equation 1. For the high-luminosity state spectrum, if  $i = 69.5^\circ$ , then  $R_{in} = 10.9 \pm 2.6$  km. The value of  $r_{ms}$  for a maximally rotating  $7M_\odot$  black hole is 10.4 km so that the value of  $R_{in}$  is consistent with a maximally rotating black hole (Bardeen, Press, & Teukolsky 1972).

We have considered the possibility that  $R_{in}$  is being underestimated because the inclination angle of the disk close to the black hole is larger than  $69.5^\circ$ . Although the binary inclination angle has been measured by Orosz & Bailyn (1997) to very high accuracy,  $i = 69.50 \pm 0.08$  degrees, it is possible that the inclination angle of the accretion disk close to the black hole is different from the binary inclination. If we assume that the inclination of the radio jets,  $85^\circ$  (Hjellming & Rupen 1995), gives the disk inclination close to the black hole, then the implied value of  $R_{in}$  increases to  $21.9 \pm 5.2$  km. Assuming that  $r_{ms} = R_{in}$  gives  $a_* = 0.93^{+0.05}_{-0.08}$ .

Timing analysis has been performed for both of the RXTE observations of GRO J1655–40 discussed in this paper, and a complete description of this analysis will be published separately (Remillard et al. 1998). A QPO at 300 Hz was observed when the source was in the high-luminosity state but not when it was in the intermediate-luminosity state. The presence of the 300 Hz QPO in the high-luminosity state may signify an important difference between the states. While, at present, there is no consensus regarding the physical mechanism generating the QPO, most of the suggested mechanisms require an accretion disk terminated near the marginally stable orbit. If 300 Hz corresponds to an orbital period around a  $7M_\odot$



black hole (Remillard et al. 1997), then the implied radius of the orbit is 64 km. This radius (64 km) is considerably more than the value of  $R_{in}$  implied by our spectral results, which probably indicates that 300 Hz is not equal to the frequency of a particle orbit at the inner edge of the disk. Other mechanisms have been suggested which may be able to explain the presence of the 300 Hz QPO in GRO J1655-40. The QPO in GRO J1655-40 may be caused by g-mode oscillations of the accretion disk (Nowak & Wagoner 1992) or by frame-dragging (Cui, Zhang, & Chen 1998a). Frame-dragging may be able to produce QPOs by causing precession of the inner region of the accretion disk (Stella & Vietri 1998).

. For both of these mechanisms, the predicted QPO frequency depends on the black hole rotation rate. Coincidentally, in both cases, a value of  $a_* = 0.95$  is derived when the models are applied to GRO J1655-40 (Zhang et al. 1997b; Cui, Zhang, & Chen 1998a). The high black hole rotation rate is in rough agreement with our spectral results.

## 5.2. Model 2 Implications

The physical picture for Model 2 is that the soft emission from the disk is Comptonized in a plasma near the disk. The high-luminosity state fit parameters imply a plasma with a temperature of  $2.66^{+0.42}_{-0.31}$  keV and an optical depth of  $7.64^{+0.75}_{-0.65}$ , which corresponds to a Comptonization y-parameter of 1.22. After the transition to the intermediate-luminosity state, the plasma temperature decreases to  $1.260^{+0.021}_{-0.026}$  keV, and the optical depth increases to  $14.11^{+1.02}_{-0.70}$ , which corresponds to  $y = 1.96$ . If the emission responsible for the iron line is Comptonized, then a broad iron line, as we observe in the GRO J1655-40 spectrum, is expected (Sunyaev & Titarchuk 1980). From the expression,  $\Delta E = (E^2 \tau^2)/m_e c^2$  (Sunyaev & Titarchuk 1980), the width of the high-luminosity state iron line gives  $\tau \sim 5.0$ . This is in reasonably good agreement with the value for  $\tau$  found from the Comptonization fit parameters for the high-luminosity state. The centroid energy of the iron line is expected to be redshifted due to the recoil of the electron since the plasma temperature of the Comptonizing region is less than the energy of the line. Our measured centroid energy is consistent with a redshifted 6.4 keV iron line but the uncertainty is too large to make a meaningful redshift estimate. There is some precedent for broad iron lines in black hole candidates. The mass of the compact object in 4U 1543-47 is between 2.5 and 7.5  $M_\odot$  (Orosz et al. 1998), indicating that it is likely that this source contains a black hole. During EXOSAT observations of 4U 1543-47, an iron line was detected with  $\sigma_{line} = 1.15$  keV and  $E_{line} = 5.93$  keV (van der Woerd, White, & Kahn 1989). Assuming that Comptonization is responsible for the broadening of the iron line, an optical depth between 4 and 5 is implied.

## 6. Conclusions

We find that the GRO J1655-40 energy spectrum can change significantly on relatively short timescales. The luminosity changes from about 18% of  $L_{edd}$  to about 10% of  $L_{edd}$ , and the photon index of the power-law component changes from  $2.72^{+0.03}_{-0.08}$  to  $2.415 \pm 0.011$  between the high and intermediate-luminosity states. Comparing the high and intermediate-luminosity state spectra shows a positive correlation between the power-law index and the flux of the power-law component, which is consistent with the previously reported trend. Models to explain the hard spectral component are constrained by this trend and the fact that power-law extends to 800 keV without a cutoff. In the high-luminosity state, we find evidence for a broad iron line and a reflection component. In the intermediate-luminosity state, there is evidence for a

broad iron line. The fact that a 300 Hz QPO is observed only in the high-luminosity state should provide additional information about the system.

We regard the models we use for the soft-component as approximations to the actual physical system. Global models of the accretion flow, which account for all of the accretion physics, are necessary. Specifically, for GRO J1655–40, it seems that the large changes in the power-law flux observed between the high-luminosity and intermediate-luminosity states must be related to the simultaneous changes in the soft component. Construction of a physical model which generates all the observed emission components and reproduces the correlation between the various spectral components will be necessary for reliable extraction of the physical parameters of accreting compact objects.

J.A.T. would like to thank D.E. Gruber and the HEXTE group at UCSD for assistance with the HEXTE deadtime correction and K. Leighly for useful comments and discussions. We also thank R.M. Hjellming and R. Hunstead for providing the results of GRO J1655–40 radio observations.

## REFERENCES

- Bardeen, J.M., Press, W.H., & Teukolsky, S.A. 1972, ApJ 178, 347
- Chakrabarti, S.K. & Titarchuk, L. 1995, ApJ 455, 623
- Cui, W., Zhang, S.N., & Chen, W. 1998a, ApJ 492, L53
- Cui, W., Ebisawa, K., Dotani, T., & Kubota, A. 1998b ApJ 493, L75
- Grandi, P., Tagliaferri, G., Giommi, P., Barr, P., Palumbo, G.G.C. 1992, ApJS 82, 93
- Grove, J.E., Johnson, W.N., Kroeger, R.A., McNaron-Brown, K., Skibo, J.G., Philips, B.F. 1998, astro-ph/9802242
- Guainazzi, M., Mihara, T., Otani, C., Matsuoka, M. 1996, PASJ 48, 781
- Haardt, F., Maraschi, L. & Ghisellini, G. 1997, ApJ 476, 620
- Hjellming, R.M. & Rupen, M.P. 1995, Nature 375, 464
- Jahoda, K. et al. 1997, XTE-PCA, <http://heawww.gsfc.nasa.gov/docs/xray/xte/pca>
- Koyama, K. et al. 1984, PASJ 36, 659
- Kroeger, R.A., Strickman, M.S., Grove, J.E., Kaaret, P., Ford, E., Harmon, B.A., McConnell, M. 1997, A&AS 120, 117
- Magdziarz, P. & Zdziarski, A.A. 1995, MNRAS 273, 837
- Makishima, K. et al. 1986, ApJ 308, 635
- Nagase, F., Inoue, H., Kotani, T., & Ueda, Y. 1994, IAUC 6094
- Nowak, M.A. & Wagoner, R.V. 1992, ApJ 393, 697
- Orosz, J.A. et al. 1998, astro-ph/9712018
- Orosz, J.A. & Bailyn, C.D. 1997, ApJ 477, 876
- Pringle, J.E. 1981, ARA&A 19, 137
- Remillard, R.A., Morgan, E.H., McClintock, J.E., Bailyn, C.D., Orosz, J.A., & Greiner, J. 1997, in *procs. Eighteenth Texas Symposium on Relativistic Astrophysics*, (World Scientific), eds. A. Olinto, J. Frieman, & D. Schramm, 750
- Remillard, R.A., Morgan, E.H., McClintock, J.E., Bailyn, C.D., & Orosz, J.A. 1998, ApJ, in press; astro-ph/9806049
- Rothschild, R.E. et al. 1997, astro-ph/9710328
- Schattenburg, M.L. & Canizares, C.R. 1986, ApJ 301, 759
- Shafer, R.A. et al. 1991, XSPEC User's Guide
- Shapiro, S.L. & Teukolsky, S.A. 1983, *Black Holes, White Dwarfs, and Neutron Stars* (New York: Wiley)

- Shimura, T. & Takahara, F. 1995, ApJ 445, 780
- Shrader, C. & Titarchuk, L. 1998, astro-ph/9803309
- Stark, M. et al. 1997, PCABACKEST, <http://lheawww.gsfc.nasa.gov/docs/xray/xte/pca>
- Stella, L. & Rosner, R. 1984, ApJ 277, 312
- Stella, L. & Vietri, M. 1998, ApJ 492, L59
- Sunyaev, R.A. & Titarchuk, L.G. 1980, A& A 86, 121
- Tavani, M., Fruchter, A., Zhang, S.N., Harmon, B.A., Hjellming, R.N., Rupen, M.P., Bailyn, C., & Livio, M. 1996, ApJ 473, L103
- Tingay, S.J. et al. 1995, Nature 374, 141
- Titarchuk, L. 1994, ApJ 434, 570
- Tomsick, J.A., Lapshov, I., & Kaaret, P. 1998, ApJ 494, 747
- Tomsick, J.A. & Kaaret, P. 1998, PCA PILE-UP, <http://lheawww.gsfc.nasa.gov/docs/xray/xte/pca>
- Toor, A. & Seward, F.D. 1974, A.J. 79, 995
- Turner, M.J.L. et al. 1989, PASJ 41, 345
- Ueda, Y., Inoue, H., Tanaka, Y., Ebisawa, K., Nagase, F., Kotani, T., Gehrels, N. 1998 ApJ 492, 782
- van der Woerd, H., White, N.E., & Kahn, S.M. 1989, ApJ 344, 320
- Wilson, C.A., Harmon, B.A., Zhang, S.N., Paciesas, W.S., Fishman, G.J. 1995, IAUC 6152
- Wilson, A.S. & Colbert, E.J.M. 1995, ApJ 438, 62
- Yaqoob, T. 1992, MNRAS 258, 198
- Zhang, S.N., Wilson, C.A., Harmon, B.A., Fishman, G.J., Wilson, R.B., Paciesas, W.S., Scott, M., & Rubin, B.C. 1994, IAUC 6046
- Zhang, S.N., Harmon, B.A., Paciesas, W.S., Fishman, G.J. 1995, IAUC 6209
- Zhang, S.N., Ebisawa, K., Sunyaev, R., Ueda, Y., Harmon, B.A., Sazonov, S., Fishman, G.J., Inoue, H., Paciesas, W.S., Takahashi, T. 1997a, ApJ 479, 381
- Zhang, S.N., Cui, W., & Chen, W. 1997b, ApJ 482, 155

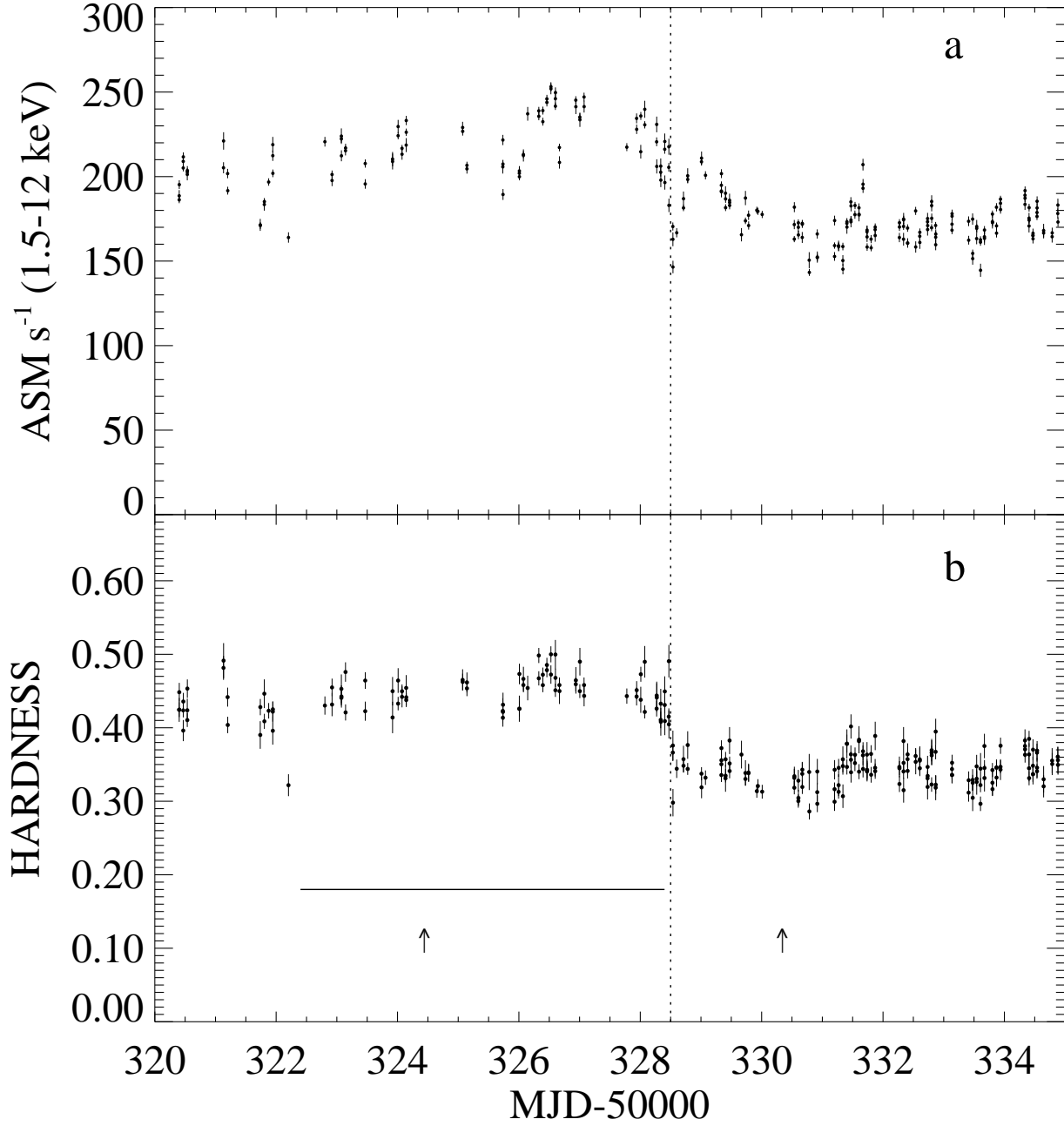


Fig. 1.— (a) The ASM 1.5-12 keV light curve for GRO J1655-40 and (b) the (5-12 keV)/(1.5-5 keV) hardness ratio vs. time. The solid horizontal line marks the time of the OSSE observation, and the arrows mark the two pointed RXTE observations. The vertical dotted line marks the transition time.

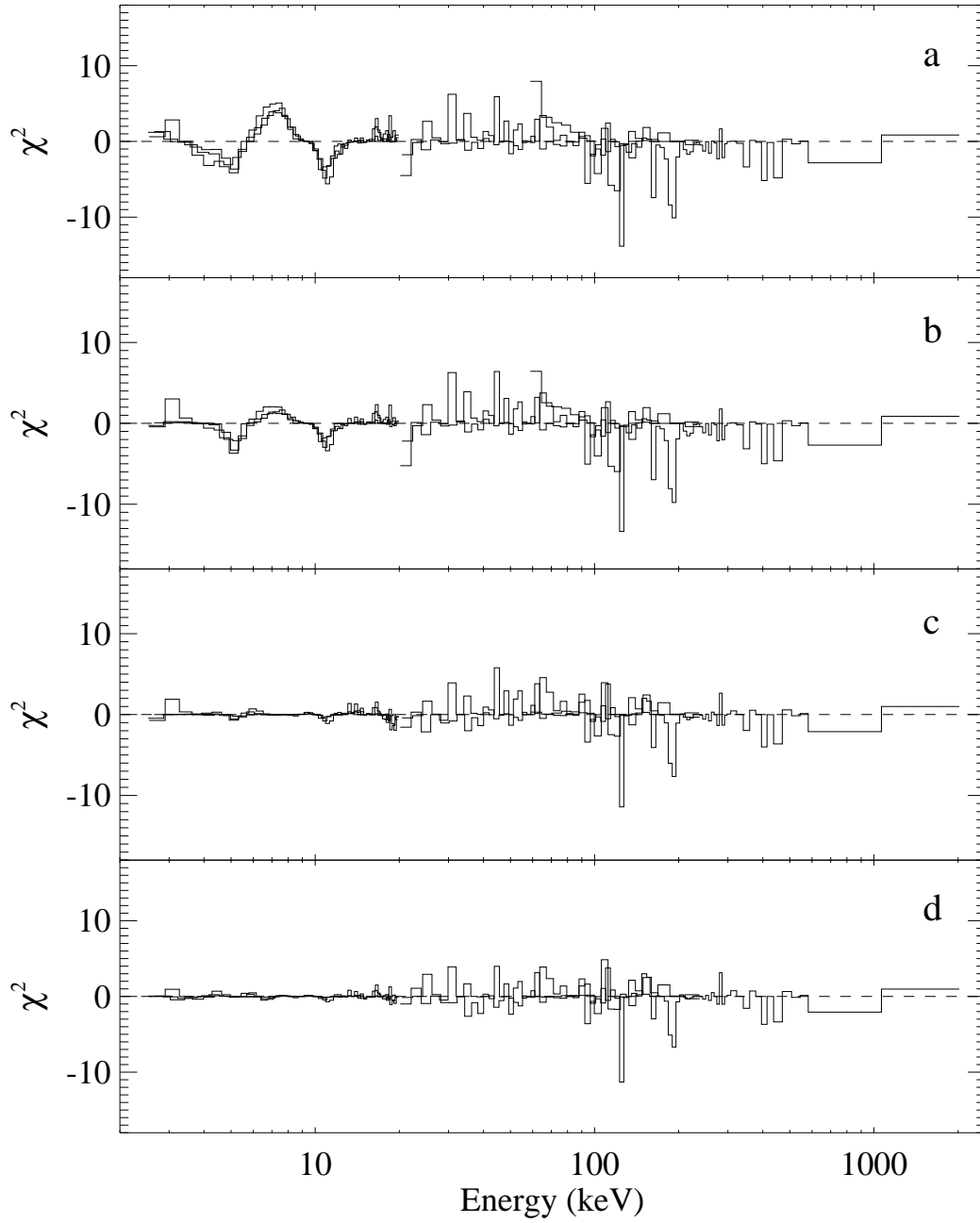


Fig. 2.— Residuals for fits to the GRO J1655–40 pre-transition spectrum. The four plots show, (a) the residuals for a disk-blackbody plus power-law fit to the GRO J1655–40 spectrum, (b) the residuals for a Comptonization plus power-law fit, (c) the residuals for a disk-blackbody plus gaussian plus power-law plus reflection fit, (d) the residuals for a Comptonization plus gaussian plus power-law plus reflection fit.

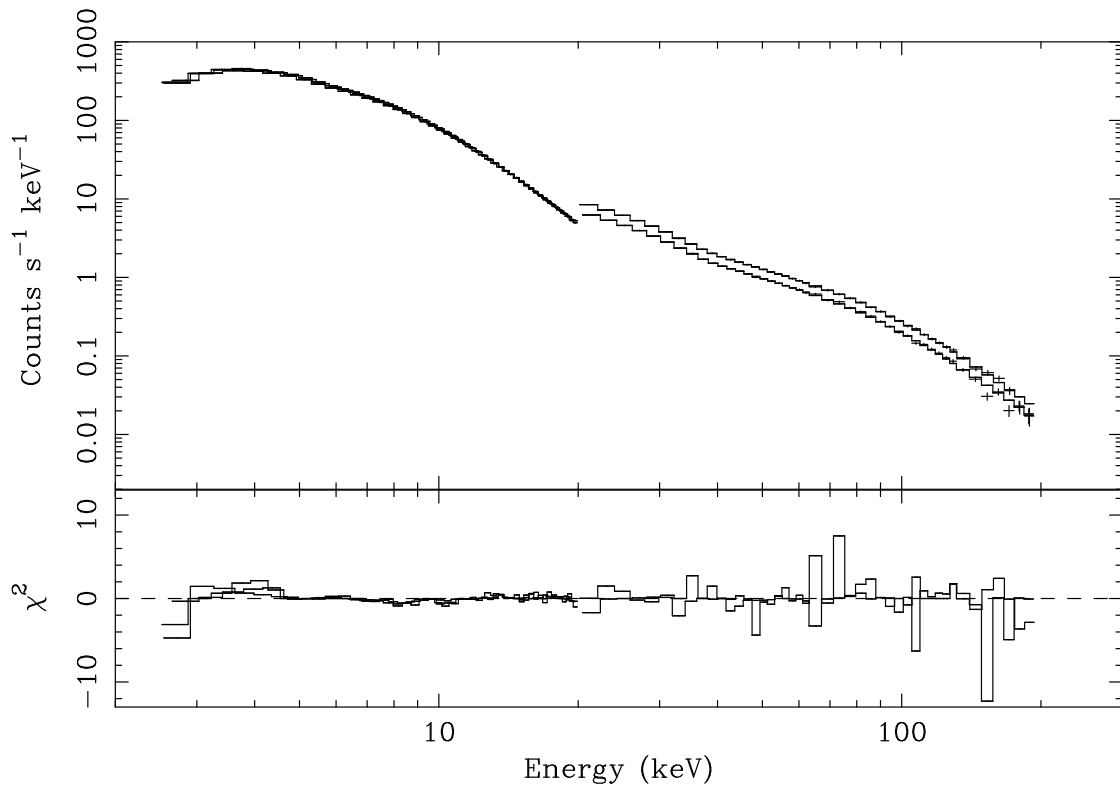


Fig. 3.— PCA (layer 1 only) and HEXTE Crab spectrum fit with a broken power-law model.

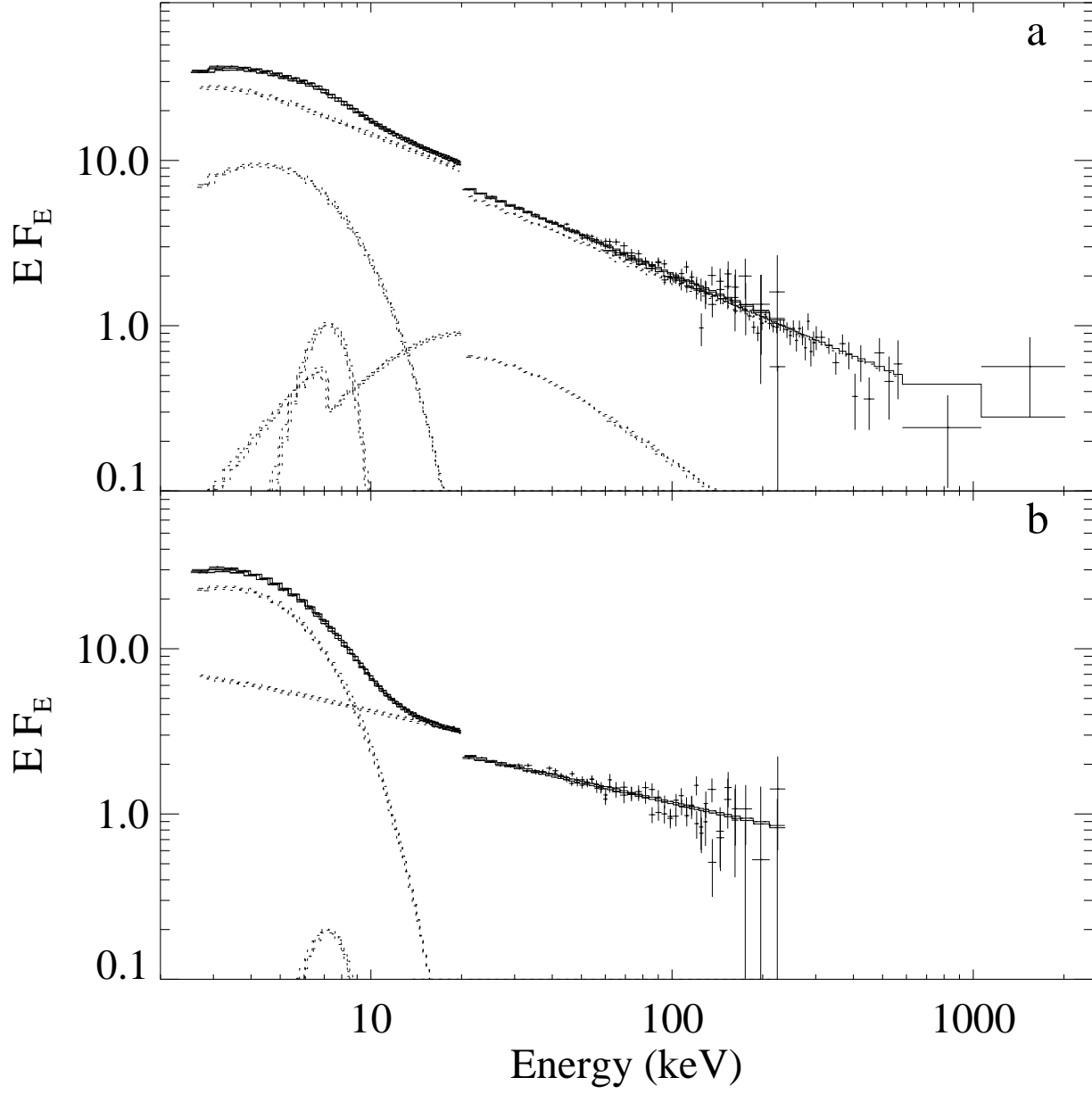


Fig. 4.— (a) and (b) show the pre-transition and post-transition GRO J1655–40 spectra, respectively. In each plot, the solid line is the Model 1 fit to the data, and the dashed lines show the Model 1 spectral components. No normalization correction has been made.



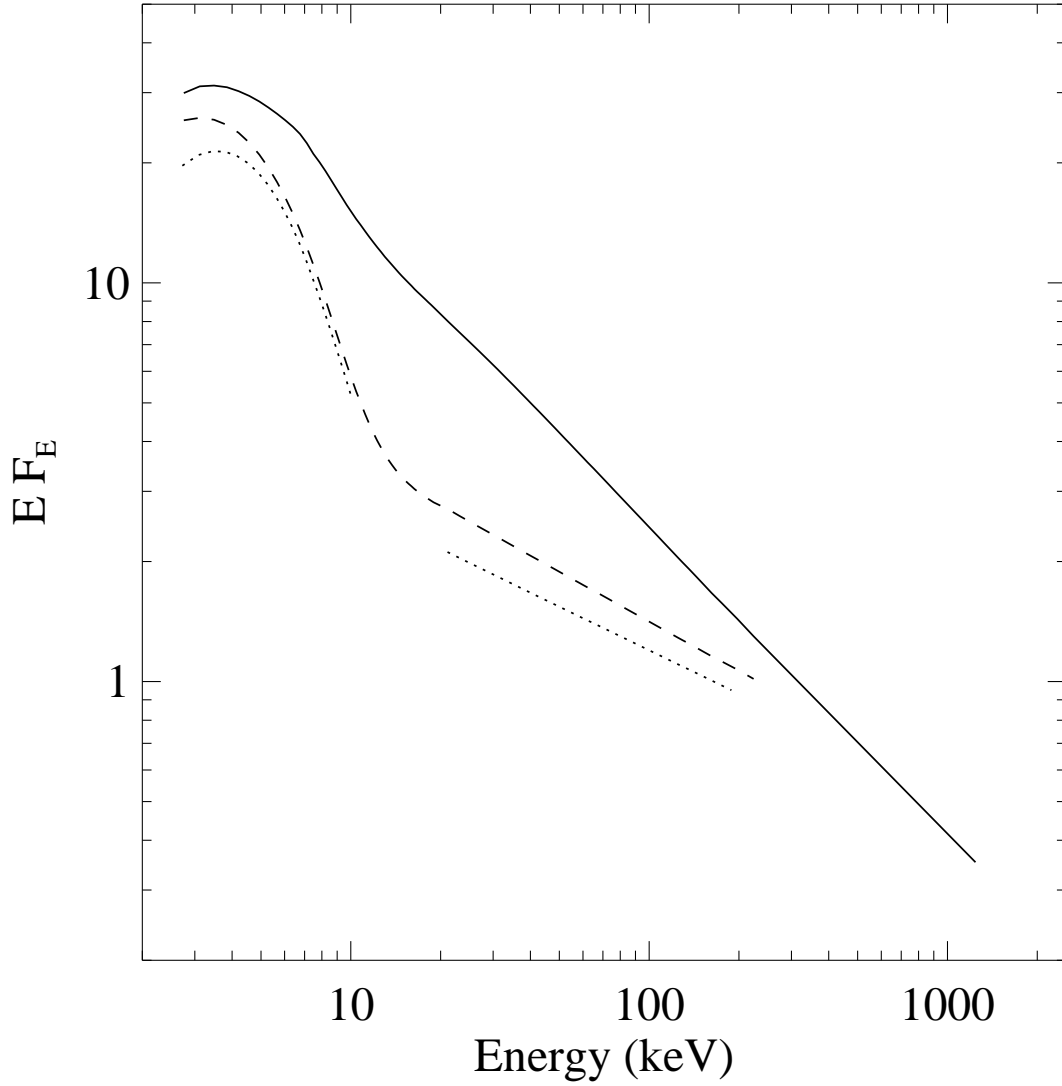


Fig. 5.— GRO J1655–40 broad-band spectra. The solid line is the Model 1 fit to the high-luminosity spectrum, the dashed line is the Model 1 fit to the intermediate-luminosity spectrum, and the dotted line is the spectrum from an August 1995 ASCA and BATSE observation of GRO J1655–40 based on the fit parameters given in Zhang et al. (1997a).

Table 1. Fits to the HEXTE and OSSE Pre-Transition Spectrum

Power-law	
$\alpha$	$2.758 \pm 0.005$
$\chi^2/\nu$	197/140
Cutoff Power-law	
$\alpha$	$2.703 \pm 0.010$
$E_f$ (keV)	$1086^{+195}_{-145}$
$\chi^2/\nu$	149/139
Power-law with Reflection	
$\alpha$	$2.739 \pm 0.006$
$\Omega/2\pi$	$0.396 \pm 0.065$
$\chi^2/\nu$	147/139
Broken Power-law	
$\alpha_1$	$2.727^{+0.007}_{-0.010}$
$E_b$ (keV)	$63^{+9}_{-14}$
$\alpha_2$	$2.818 \pm 0.013$
$\chi^2/\nu$	144/138

Table 2.  $\chi^2$  values for the disk-blackbody (DBB) fits

Model	$\chi^2/\nu$ (Pre-Transition)	$\chi^2/\nu$ (Post-Transition)
DBB+power-law	391/274	187/221
DBB+power-law+reflection	244/273	187/220
DBB+gaussian+power-law	220/271	175/218
DBB+gaussian+power-law+reflection	191/270	175/217

Table 3.  $\chi^2$  values for the Comptonization (COMP) fits

Model	$\chi^2/\nu$ (Pre-Transition)	$\chi^2/\nu$ (Post-Transition)
COMP+power-law	291/273	188/220
COMP+power-law+reflection	229/272	188/219
COMP+gaussian+power-law	218/270	155/217
COMP+gaussian+power-law+reflection	171/269	155/216

Table 4. GRO J1655–40 spectral fits with Model 1<sup>a</sup>

Parameter	Pre-transition <sup>b</sup>	Post-transition <sup>c</sup>
$N_{\text{H}}$ ( $10^{22}$ H atoms $\text{cm}^{-2}$ )	$1.803^{+0.084}_{-0.089}$	$0.372 \pm 0.055$
Disk-Blackbody		
$kT_{max}$ (keV)	$1.489^{+0.023}_{-0.026}$	$1.227 \pm 0.004$
$N_{DBB}$	$49.0 \pm 2.7$	$245.8 \pm 4.2$
Flux (photons $\text{cm}^{-2}$ $\text{s}^{-1}$ ) <sup>d</sup>	2.39	5.00
Power-law		
$\alpha$	$2.747 \pm 0.006$	$2.416 \pm 0.009$
Flux (photons $\text{cm}^{-2}$ $\text{s}^{-1}$ ) <sup>d</sup>	$7.98 \pm 0.23$	$1.742 \pm 0.049$
Gaussian		
$E_{line}$ (keV)	$6.81^{+0.24}_{-0.31}$	$6.81^e$
$\sigma_{line}$ (keV)	$1.21^{+0.20}_{-0.18}$	$1.21^e$
$N_{line}$ (photons $\text{cm}^{-2}$ $\text{s}^{-1}$ )	$0.057^{+0.022}_{-0.015}$	$0.0107 \pm 0.0036$
EW (eV)	113	38
Reflection		
$\Omega/2\pi$	$0.259^{+0.054}_{-0.053}$	$0.0^e$
$i^e$	$69.5^{\circ}$	-
$\chi^2/\nu$	191/270	178/220

<sup>a</sup>The errors are 68% confidence for one interesting parameter ( $\Delta\chi^2 = 1.0$ ).

<sup>b</sup>Fit includes data from the PCA, HEXTE, and OSSE.

<sup>c</sup>Fit includes data from the PCA and HEXTE.

<sup>d</sup>This is the unabsorbed 2.5-20 keV component flux.

<sup>e</sup>Fixed.

Table 5. GRO J1655–40 spectral fits with Model 2<sup>a</sup>

Parameter	Pre-transition <sup>b</sup>	Post-transition <sup>c</sup>
$N_{\text{H}}$ ( $10^{22}$ H atoms $\text{cm}^{-2}$ )	$2.99^{+0.18}_{-0.16}$	$2.57^{+0.30}_{-0.39}$
Comptonization		
$kT$ (keV)	$2.66^{+0.42}_{-0.31}$	$1.260^{+0.021}_{-0.026}$
$\tau$	$7.64^{+0.75}_{-0.65}$	$14.11^{+1.02}_{-0.70}$
Flux (photons $\text{cm}^{-2}$ $\text{s}^{-1}$ ) <sup>d</sup>	$5.7 \pm 1.4$	$6.7^{+1.2}_{-1.3}$
Power-law		
$\alpha$	$2.691^{+0.023}_{-0.056}$	$2.414 \pm 0.010$
Flux (photons $\text{cm}^{-2}$ $\text{s}^{-1}$ ) <sup>d</sup>	$5.7^{+1.1}_{-1.9}$	$2.050^{+0.059}_{-0.053}$
Gaussian		
$E_{\text{line}}$ (keV)	$6.21^{+0.31}_{-0.33}$	$6.21^{\text{e}}$
$\sigma_{\text{line}}$ (keV)	$1.69^{+0.16}_{-0.15}$	$1.69^{\text{e}}$
$N_{\text{line}}$ (photons $\text{cm}^{-2}$ $\text{s}^{-1}$ )	$0.203^{+0.054}_{-0.039}$	$0.077^{+0.013}_{-0.016}$
EW (eV)	319	192
Reflection		
$\Omega/2\pi$	$0.85^{+0.68}_{-0.25}$	$0.0^{\text{e}}$
$i^{\text{e}}$	$69.5^{\circ}$	-
$\chi^2/\nu$	171/269	159/219

<sup>a</sup>The errors are 68% confidence for one interesting parameter ( $\Delta\chi^2 = 1.0$ ).

<sup>b</sup>Fit includes data from the PCA, HEXTE, and OSSE.

<sup>c</sup>Fit includes data from the PCA and HEXTE.

<sup>d</sup>This is the unabsorbed 2.5-20 keV component flux.

<sup>e</sup>Fixed.